

# A FEM-DEM model for immersed granular flows: from unresolved to semi-resolved scales

Michel Henry<sup>1,\*</sup>, Laura Valentina Cote Martinez<sup>2,\*\*</sup>, Cristina Jommi<sup>2,3,\*\*\*</sup>, Michael Hicks<sup>2,\*\*\*\*</sup>, Jonathan Lambrechts<sup>1,†</sup>, Vincent Legat<sup>1,‡</sup>, and Miguel Cabrera<sup>2,§</sup>

<sup>1</sup>Université Catholique de Louvain, Belgium

<sup>2</sup>Delft University of Technology, The Netherlands

<sup>3</sup>Politecnico di Milano, Italy

**Abstract.** This work presents a coupling between the Finite Element Method (FEM) and the Discrete Element Method (DEM) to simulate immersed granular flows, transitioning from an unresolved to a semi-resolved representation. This refers to fluid discretisations ranging from a scale much larger than the grain size to one comparable to the grain size. The fluid phase is modelled using the Volume-Averaged Navier-Stokes (VANS) equations, which are solved with the FEM, while the granular phase is represented by the DEM with Non-Smooth Contact Dynamics (NSCD). An overlap-wise spatial coupling is proposed to bridge the gap between unresolved and semi-resolved scales. The method is validated by numerically reproducing experimental work on the fluidisation of a sand layer. Accuracy and stability are assessed by varying the mesh size down to half the grain diameter.

## 1 Introduction

Immersed granular flows refer to the motion of a granular material in a fluid. These flows are ubiquitous in nature and industry, from landslides to fluidised beds. The discrete nature of the grains makes the modeling of these flows challenging, as the fluid and solid phases interact at different scales. Classical Computational Fluid Dynamics (CFD) methods are used to model the fluid phase, while the Discrete Element Method (DEM) is used to track the grains within a Lagrangian formulation to allow direct observation of the grain behavior. A comprehensive review of the numerical methods available for immersed granular flows is provided by Zhao [1]. Depending on the mesh size to grain diameter ratio, CFD-DEM are classified as resolved or unresolved. The resolved approach assumes the mesh size at least ten times smaller than the grain diameter in order to capture the interface between the two phases. Fluid-structure interaction models are then used to account for the local interactions between the fluid and the grains, such as the immersed boundary method or the fictitious domain method. The unresolved approach, on the other hand, assumes a mesh size at least three times larger than the grain diameter. Constitutive laws are introduced to account for the local interactions between the fluid and the grains without the need to resolve the grain geometry. The in-between discretization region is referred to as the semi-resolved approach [2, 3].

In this work, we present a methodology for bridging the gap between unresolved and semi-resolved approaches based on the weak form of the Volume-Averaged Navier-Stokes equations

(VANS) equations. The fluid phase is described at a macroscopic level by the VANS [4]. A drag force is introduced to account for the momentum exchange between the fluid and the grains [5, 6]. The void fraction acts as a smooth indicator function to account for the presence of the grains in the fluid which satisfy the volume conservation equation. An accurate representation of the void fraction is crucial to capture the local interactions between the fluid and the grains [7]. In this paper, an exact particle-wise integration of the void fraction is performed enabling a low void fraction resolution [8]. To integrate exactly a linear function over the particles, the centroid of the overlap between the particles and each mesh cell is computed. A semi-implicit scheme is used to couple the fluid and the grains while ensuring the stability of the system even for low void fraction resolution. This methodology is validated against the fluidisation of a granular layer test case presented by [9]. The mesh sensitivity is investigated to ensure the accuracy of results.

## 2 One Model, Two Scales

To bridge the gap between a element mesh size larger than a grain – unresolved approach – to an element mesh size comparable to grain size – semi-resolved approach [10, 11] – an exact particle spatial integration over the underlying mesh elements is proposed. The governing equations for fluid-grain dynamics and the required constitutive laws are first recalled in Sec. 2.1. The particle based spatial discretization is then presented Sec. 2.2, followed by the time integration coupling scheme in Sec. 2.3. This framework provides a unified and consistent description of fluid-grain interactions across different resolution levels.

### 2.1 Fluid-Grain Dynamics

The governing equations at the unresolved and semi-resolved scale are obtained by filtering the Navier-Stokes equations over a

\*e-mail: michel.henry@uclouvain.be

\*\*e-mail: l.cotemartinez@tudelft.nl

\*\*\*e-mail: c.jommi@tudelft.nl

\*\*\*\*e-mail: m.a.hicks@tudelft.nl

†e-mail: jonathan.lambrechts@uclouvain.be

‡e-mail: vincent.legat@uclouvain.be

§e-mail: m.a.cabrera@tudelft.nl

control volume incorporating grains, while imposing the velocity continuity at the fluid-grain interface. The resulting Equations (1)–(2), are the VANS equations:

$$\nabla \cdot (\varepsilon \mathbf{u} + (1 - \varepsilon) \mathbf{v}) = 0, \quad (1)$$

$$\varepsilon \rho \frac{d\mathbf{u}}{dt} = \nabla \cdot \boldsymbol{\sigma} + \varepsilon \rho \mathbf{g} + (1 - \varepsilon) \mathbf{f}, \quad (2)$$

where  $\mathbf{u}$  is the fluid velocity,  $\mathbf{v}$  is the averaged solid velocity,  $\rho$  is the fluid density,  $\boldsymbol{\sigma}$  is the Cauchy stress tensor,  $\mathbf{g}$  is the gravitational acceleration,  $\varepsilon$  is the void fraction and  $\mathbf{f}$  is the fluid-grain interaction force. The material derivative is defined as  $\frac{d\bullet}{dt} = \frac{\partial\bullet}{\partial t} + \mathbf{u} \cdot \nabla\bullet$ . The stress tensor is defined as

$$\boldsymbol{\sigma} = -p\mathbf{I} + \varepsilon\eta(\nabla\mathbf{u} + \nabla^T\mathbf{u}), \quad (3)$$

where  $p$  is the pressure,  $\mathbf{I}$  is the identity tensor, and  $\eta$  is the dynamic viscosity. Equations (1)–(2) are solved using the Finite Element Method (FEM) with a stabilised mixed formulation with  $\mathbb{P}_1$ – $\mathbb{P}_1$  elements for velocity–pressure. The implementation has been carried out in our in-house code, MigFlow [12–15].

Each grain is assumed to be a circular rigid body with a prescribed radius and mass. Its motion is governed by the Newton-Euler equations, and contacts with other bodies are obtained by the Non-Smooth Contact Dynamics (NSCD) :

$$\frac{d\mathbf{x}}{dt} = \mathbf{v}, \quad (4)$$

$$m \frac{d\mathbf{v}}{dt} = m\mathbf{g} + \mathbf{F} + \mathbf{F}_c, \quad (5)$$

$$I \frac{d\boldsymbol{\omega}}{dt} = \mathbf{M} + \mathbf{M}_c, \quad (6)$$

where  $m$  is the mass,  $\mathbf{x}$  is the position,  $\mathbf{v}$  is the grain velocity,  $I$  is the moment of inertia,  $\boldsymbol{\omega}$  is the angular velocity,  $\mathbf{F}$  is the fluid-grain force,  $\mathbf{F}_c$  is the contact force,  $\mathbf{M}$  is the fluid-grain torque and  $\mathbf{M}_c$  is the contact torque. NSCD determines a contact impulse that enforces the non-penetration condition between grains. A review of the method can be found in [16].

A non-linear Gauss–Seidel iterative scheme is employed to solve the global contact problem [17]. The solid time step is selected to limit the number of potential contacts during the detection phase and is defined as  $\Delta t_s \propto d_{\min}/\|v_{\max}\|$ , where  $d_{\min}$  denotes the minimum grain diameter and  $\|v_{\max}\|$  the maximum grain velocity. Any potential mismatch between the fluid and solid time steps is addressed via a sub-stepping strategy applied to the solid phase.

Lift force or the Basset history force are neglected in the present work, and only the drag force is considered; hence the fluid-grain force is given by

$$\mathbf{F} = \int_{V_p} (\nabla \cdot \boldsymbol{\sigma} + \mathbf{f}_{\text{drag}}) dV_p, \quad (7)$$

where  $V_p$  is the grain volume, and  $\mathbf{f}_{\text{drag}}$  is the drag force density. No torque is exerted on the grains by the fluid. The Dallavalle correlation with the Di Felice voidage function are used as constitutive laws for the drag force density,

$$\mathbf{f}_{\text{drag}} = \underbrace{\varepsilon^{-2.8} (0.77 \sqrt{\varepsilon \text{Re}} + 5.87)}_{\hat{\alpha}_y} \frac{\eta}{d^2} (\mathbf{u} - \mathbf{v}), \quad (8)$$

where  $d$  is the grain diameter and  $\text{Re}$  is the Reynolds number,  $\text{Re} = \rho d \|\mathbf{u} - \mathbf{v}\| / \eta$ . This constitutive law is valid for Reynolds numbers  $\text{Re} < 10^4$  and void fractions  $\varepsilon > 0.3$  [5, 18].

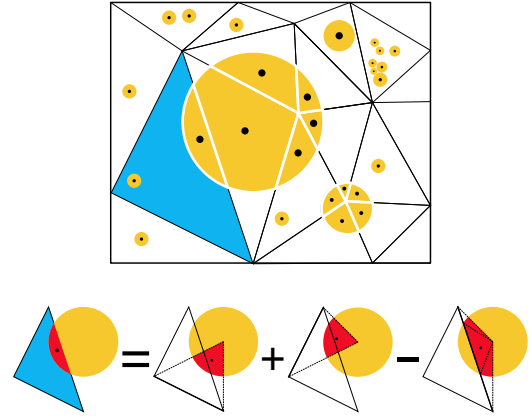


**Figure 1.** Representation of the integration scheme. Particles, in orange, are partitioned by the elements they overlap. The centroid of the overlap, in black, is used as the integration point.

## 2.2 An overlap-wise spatial coupling

The fluid phase is represented over a domain composed of both particles and fluid. Discrete fields are related to their continuous volume-averaged representation, within the finite element formulation, as follows:

$$\int_V (1 - \varepsilon) \phi dV = \sum_p \int_{V_p} \phi dV_p, \quad (9)$$

$$\int_V (1 - \varepsilon) \mathbf{v} \cdot \nabla \phi dV = \sum_p \int_{V_p} \mathbf{v} \cdot \nabla \phi dV_p, \quad (10)$$

$$\int_V (1 - \varepsilon) \mathbf{f} \phi dV = - \sum_p \int_{V_p} (\nabla \cdot \boldsymbol{\sigma} + \mathbf{f}_{\text{drag}}) \phi dV_p, \quad (11)$$

where  $V$  is the mixture volume,  $\phi$  is the test function,  $\mathbf{v}$  the averaged solid velocity, and  $\mathbf{f}$  the fluid-grain interaction force. Equation (9) is mass-lumped in order to maintain a continuous bounded void fraction between 0 and 1. The left-hand side of Equations (10)–(11), which appears in the weak form of the problem, Equations (1)–(2), is replaced by the corresponding right-hand side expressions. The resulting integral is then evaluated by partitioning the grains according to the mesh elements they overlap, and using the centroids of these overlap regions as integration points. Figure 1 illustrates how to compute the overlap area and centroid of an element. This integration rule exactly integrates linear functions over the grains. Additionally, it naturally smooths the local force to all intersected elements.

## 2.3 A semi-implicit CFD-DEM scheme

In the previous section, the spatial discretisation has been discussed, and it is now necessary to address the temporal discretisation. A linearisation of the VANS equations is performed. The void fraction is computed explicitly based on the current grain position. Advection terms are treated with a semi-implicit scheme, while stress terms are treated implicitly. The fluid-grain interaction force is treated with a semi-implicit scheme:

$$\nabla \cdot (\varepsilon \mathbf{u}^{n+1} + (1 - \varepsilon) \mathbf{v}^*) = 0, \quad (12)$$

$$\varepsilon \rho \left( \frac{\mathbf{u}^{n+1} - \mathbf{u}^n}{\Delta t} + \mathbf{u}^n \cdot \nabla \mathbf{u}^{n+1} \right) = \nabla \cdot \boldsymbol{\sigma}^{n+1} + \varepsilon \rho \mathbf{g} + (1 - \varepsilon) \mathbf{f}^*, \quad (13)$$

where  $n$  refers to the explicit value,  $n + 1$  refers to the implicit value, and  $*$  refers to the semi-implicit value. To compute the semi-implicit value, the grain velocity is predicted using Equation 5, resulting in:

$$m \frac{\mathbf{v}^* - \mathbf{v}^n}{\Delta t} = m\mathbf{g} + \mathbf{F}_c^n + V_p \left[ -\nabla p^{n+1} + \gamma^n (\mathbf{u}^{n+1} - \mathbf{v}^*) \right], \quad (14)$$

where the fluid fields are evaluated at the integration points, *i.e.* the centroids of the overlapping elements. Note that the fluid–grain interaction is assumed to consist solely of the pressure gradient and drag forces. The grain velocity, Equation 15, is predicted as

$$\mathbf{v}^* = \left[ \frac{m}{\Delta t} + \gamma^n \right]^{-1} \left[ \frac{m}{\Delta t} \mathbf{v}^n + m\mathbf{g} + \mathbf{F}_c^n + V_p \left( -\nabla p^{n+1} + \gamma^n \mathbf{u}^{n+1} \right) \right] \quad (15)$$

The prediction is then used to compute the fluid–grain interaction force, Equation 11, and the averaged solid velocity, Equation 10. At low void fractions, the momentum is dominated by the drag force and the continuity equation is stabilised by the prediction of the solid velocity.

### 3 Fluidisation of a granular layer

A granular layer is subjected to an increasing bottom pressure, leading to loosening of the soil. To investigate the influence of the particle spatial coupling, the experimental apparatus of [9] is numerically simulated for different mesh sizes. The differential head for the first movement and the total heave are measured and compared to the experimental data. The head is defined as

$$\psi = y + \frac{p}{\rho g} + \frac{\|\mathbf{u}\|^2}{2g}, \quad (16)$$

where  $y$  is the vertical position,  $p$  is the pressure,  $\mathbf{u}$  is the fluid velocity, and  $g$  is the gravity acceleration. The differential head is measured between the bed top and bottom. The first movement is defined as the instant when grains start to be lifted. The total heave, on the other hand, is defined as the instant when the whole bed is lifted. These definitions do not provide a rigorous mathematical definition; therefore we have chosen to define them in terms of the grain motion. A grain is considered to be in motion if it has moved more than a threshold, set to be the maximum grain diameter. The first movement is then defined when at least 5% of the grains (in terms of mass) are in motion. The total heave is defined once 95% of the grains are in motion.

The granular system consists of slightly polydisperse discs, defined by the size span  $\lambda = d_{\max}/d_{\min} = 1.2$ , with the minimum diameter set to 0.2 mm. The discs have a density  $\rho_p = 2630 \text{ kg/m}^3$ , and a friction coefficient of 0.4. An initial deposit is generated by letting the particles settle by self-weight in the rectangular domain. As the random close packing of the discs gives a larger compacity than a packing of spheres, the discs radius are reduced to match the sphere close packing. This numerical modification is only performed from the fluid side, the discrete element method still assumes the discs to be of the original size. Hence, the initial packing fraction measured in the numerical setup is equivalent to a 3D packing fraction of  $\phi_0 = 0.52$ . The ambient fluid is set to water, with density  $\rho = 1000 \text{ kg/m}^3$  and viscosity  $\eta = 0.001 \text{ Pa s}$ . The side boundaries are considered as solid and impermeable walls, a back pressure, equivalent to the

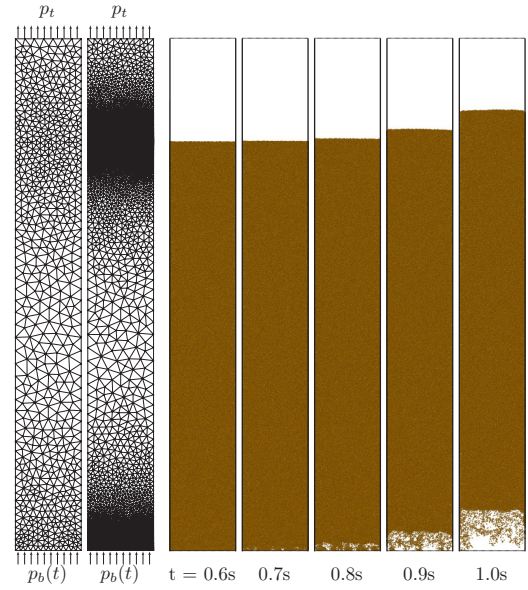


**Figure 2.** On the left, two meshes used for the simulation, the leftmost mesh refers to an unresolved case,  $h/d = 8$ , and the rightmost mesh refers to a semi-resolved case,  $h/d = 0.5$ . On the right, simulation snapshots over the latter mesh. For clarity, the fluid phase is hidden from this visualisation.

103 kPa in [9], is assigned at the top boundary and an increasing pressure input is assigned at the bottom boundary.

The fluid domain is discretised with a triangular mesh with a variable mesh size for computational efficiency. Mesh sensitivity is investigated by varying the mesh size close to the top and bottom of the bed from 0.25 to 8 times the grain diameter. Figure 2 shows the soil loosening test snapshots for a mesh ratio of 0.5.

The granular layer is initially at rest, and the bottom pressure is increased as

$$p_b(t) = p_0 + \rho g H \frac{t}{\Delta t}, \quad p_0 = p_i + \rho g H, \quad (17)$$

where  $p_b$  is the bottom pressure,  $p_0$  is the initial bottom pressure,  $p_i$  is the top pressure,  $H$  is the height of the layer, and  $\Delta t$  is the time rate set to one. As the bottom pressure increases, the differential head  $\Delta h$  increases and the particles start to move.

For each mesh considered, the instants at which the first movement and the total heave are detected are recorded. Figure 3 shows the evolution of the solid mass fraction in motion and the associated differential head. For each mesh size, the first movement is detected at  $t \approx 0.69\text{s}$  and the total heave is detected at  $t \approx 0.72\text{s}$ . The differential head for total heave is around 22 cm for all mesh sizes. This is a slight overestimation compared to the experimental data of 19 cm. This discrepancy can be attributed to the bi-dimensional nature of the simulation, as the geometrical constraints are more restrictive in a bi-dimensional setup. Therefore, the pressure required to trigger a motion must be higher than in a tri-dimensional setup.

### 4 Conclusions

A formulation for semi-resolved simulations of immersed granular flows is presented. An overlap-wise spatial coupling is proposed to bridge the gap between unresolved and semi-resolved scales. The fluid phase is described by the VANS equations, with a drag force to account for the momentum exchange between

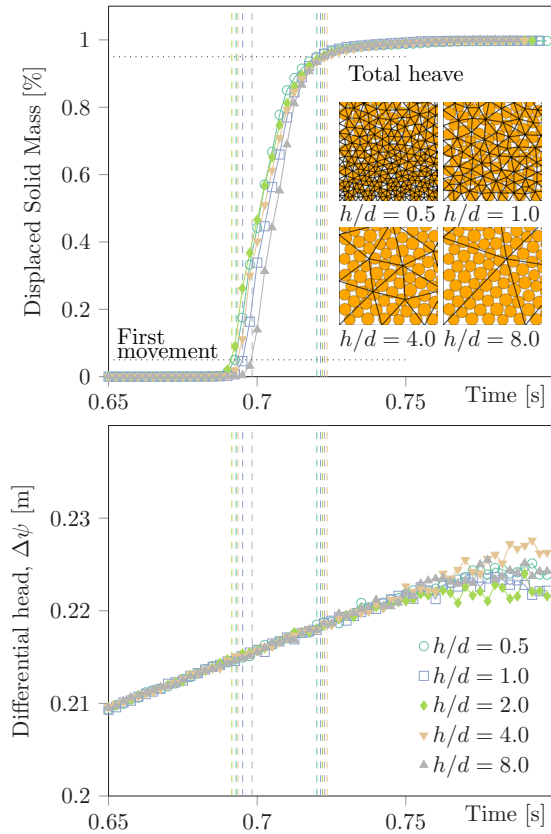


**Figure 3.** On the top, evolution of the solid mass fraction in motion for different mesh sizes. On the bottom, the differential head evolution for different mesh sizes.

the fluid and the grains. To validate the proposed methodology, the fluidisation of a granular layer case is considered. The mesh sensitivity is investigated to ensure the accuracy of the results. Both semi-resolved and unresolved approaches describes accurately the macroscopic behaviour of the granular layer. For large simulations, the unresolved approach is computationally more convenient. Still, the semi-resolved approach is more appropriate to capture local fluidisation. The overlap-wise spatial integration bridge the gap between unresolved and semi-resolved scales, providing flexibility in the choice of the simulation scale. Open questions remain regarding the drag parameterization as the drag coefficient diverges at a low void fraction. Stability is maintained by the semi-implicit coupling. Future work will focus on the extension of the methodology to include rotation coupling and investigate resolved simulation analysis within the same framework.

## References

- [1] J. Zhao, S. Zhao, S. Luding, *Nature Reviews Physics* **5**, 505 (2023).
- [2] Z. Wang, Y. Teng, M. Liu, *Journal of Computational Physics* **384**, 151 (2019).
- [3] J. Capecelatro, O. Desjardins, *Journal of Computational Physics* **238**, 1 (2013).
- [4] T.B. Anderson, R. Jackson, *Industrial & Engineering Chemistry Fundamentals* **6**, 527 (1967).
- [5] R. Di Felice, *International Journal of Multiphase Flow* **20**, 153 (1994).
- [6] J.M. DallaValle, A. Klemin (Pitman Publishing Corporation, New York ; Chicago, 1943)
- [7] D.A. Clarke, A.J. Sederman, L.F. Gladden, D.J. Holland, *Industrial & Engineering Chemistry Research* **57**, 3002 (2018).
- [8] S. Strobl, A. Formella, T. Pöschel, *Journal of Computational Physics* **311**, 158 (2016).
- [9] S. Peng, J.D. Rice, *Journal of Geotechnical and Geoenvironmental Engineering* **146**, 04020069 (2020).
- [10] T. El Geitani, B. Blais, *Industrial & Engineering Chemistry Research* **62**, 5394 (2023).
- [11] Z. Wang, M. Liu, *International Journal of Heat and Mass Transfer* **159**, 120150 (2020).
- [12] T. Leyssens, M. Henry, J. Lambrechts, V. Legat, J.F. Remacle, A coupled pfem-dem model for fluid-granular flows with free surface dynamics applied to landslides, *Journal of Computational Physics* **537**, 114082 (2025).
- [13] M. Constant, F. Dubois, J. Lambrechts, V. Legat, *Computational Particle Mechanics* (2018).
- [14] N. Coppin, M. Henry, M. Cabrera, E. Azéma, F. Dubois, V. Legat, J. Lambrechts, *Physical Review Fluids* **8**, 094303 (2023).
- [15] M. Henry, N. Coppin, S. Dorbolo, V. Legat, J. Lambrechts, *International Journal of Heat and Mass Transfer* **241**, 126755 (2025).
- [16] F. Dubois, V. Acary, M. Jean, *Comptes Rendus Mécanique* **346**, 247 (2018).
- [17] F. Jourdan, P. Alart, M. Jean, *Computer methods in applied mechanics and engineering* **155**, 31 (1998).
- [18] T. Zhao, G. Houlby, S. Utili, *Granular matter* **16**, 921 (2014).